Proceedings of ASME Turbo Expo 2011
GT2011
June 6-10, 2011, Vancouver, British Columbia, Canada

GT2011-45885

MEASUREMENT BASED ATOMIZATION MODEL FOR DIESEL SPRAY EVAPORATION AND COMBUSTION IN A MATRIX BURNER

Dieter Bohn[*]
Institute of Steam and Gas Turbines
RWTH Aachen University
Templergraben 55, 52056 Aachen
Germany
Email: post-bohn@idg.rwth-aachen.de

James Willie[†]
Institute of Steam and Gas Turbines
RWTH Aachen University
Templergraben 55, 52056 Aachen
Germany
Email: jwillie2000@gmail.com

ABSTRACT

This paper describes the development of an atomization model for implementation in a CFD solver. The model is developed for application in a matrix burner that is suitable for simulating the conditions prevailing in stationary gas turbines. The fuel considered is diesel and the matrix burner is designed using the Lean Premixed Prevaporized (LPP) concept. In this concept, the liquid fuel is first atomized, vaporized and thoroughly premixed with the oxidizer before it enters the combustion chamber. The injector used is a hollow-cone Schlick series 121-123 pressure-swirl atomizer. Extensive measurements are carried out at different atomization pressures to determine the right parameters like the nozzle diameter, atomization pressure and spray cone angle that will yield a good spray pattern. Based on the measurement data, the mass flow rate and the droplet size distribution are determined. The latter is determined by curve fitting the experimental data. The determined droplet size distribution is implemented in a Fortran subroutine that is hooked to the CFD solver. Cold flow CFD results are compared for different positions of the nozzle. The hot flow CFD results are also compared with the hot flow results obtained when the droplet size distribution is assumed to be uniform.

NOMENCLATURE

B	Pre-exponential factor	$[m^3/(kmol\,s)]$
C_p	Specific heat	$[J/(kg\,K)]$
D	Nozzle diameter	[m]
d	Droplet diameter	[μm]
d_m	Rosin-Rammler mean diameter	[μm]
E	Activation energy	[J/kmol]
F(d)	Cumulative density function	[-]
f(d)	Probability density function	$[1/\mu m]$
$\dot{m}$	Mass flow rate	[kg/s]
n	Number of droplets of diameter d	[-]
n_p	Number of particles	[-]
p	Pressure	[Pa]
Δp	Pressure drop	[Pa]
R	Universal gas constant	$[J/(kmol\,K)]$
T	Temperature	[K]
u	Velocity	[m/s]
W	Molecular weight	[kg/kmol]
Y	Species mass fraction	[-]
ρ	Density	$[kg/m^3]$
σ_s	Standard deviation	[μm]
μ	Mean	[μm]
ω	Rate of reaction	[kmol/s]
δ	Rosin-Rammler spread parameter	[-]
ν'	Reactant stoichiometric coefficient	[-]
ν''	Product stoichiometric coefficient	[-]

[*]Full Professor, Director
[†]Research Engineer

ϕ	Equivalence ratio	[-]
α_D	Flow or discharge coefficient	[-]
α	Angle nozzle axis makes with the horizontal	[°]
γ	Half-spray cone angle	[°]
β	Unmixedness parameter	[-]

INTRODUCTION

Most gas turbine combustors are designed to adhere to stringent NOx emission regulations and such emission levels can only be achieved by running combustion under lean conditions. Lean premixed pre-vaporized (LPP) combustion is advantageous because of the lower NOx emissions it produces. However, running gas turbines lean and premixed makes them exceptionally prone to combustion instabilities. A lot of work has been done in thermoacoustics, but mostly with gaseous fuels. A lot more still needs to be done with liquid fuels, especially under typical gas turbine engines conditions. The obvious reason is because of the complexities that are associated with modeling liquid fuels. The many elementary processes involve with liquid fuels makes this task challenging, especially the accurate determination of the droplet size distribution in the atomization model. Compressibility effects have to also be taken into account because of acoustics. In the work of Schuermanns et al. for example, detailed thermoacoustics approach for modeling gaseous fuel in a gas turbine burner is given [1]. The flame transfer function determined showed good agreement with that obtained from measurements. Similar work has been carried out for gaseous fuel in the matrix burner and reported in [2, 3, 4, 5]. This, however, is not the case when modeling diesel or other liquid fuels. A lot has to be done in order to accurately determine the flame transfer function and acoustic transfer matrix for liquid fuels, especially under high pressure conditions.

The matrix burner investigated in this work could handle only gaseous fuel. For it to handle liquid fuel, some design changes had to be made as reported in the work by Bohn et al. [6]. Some of the findings reported in the work include the optimum position of the nozzles together with the arrangement that gives the best fuel-air mixing. The effect of air-side forcing on the atomization process is also discussed. However, the atomization model used in this work assumed that the droplet size distribution was uniform, which does not represent the Schlick injector used in the measurements.

Liquid fuels have an obvious advantage over gaseous fuels because they are easier to handle. On the other hand, combustion involving liquid fuel is much more complicated for the obvious reason that the liquid fuel must be vaporized before it can combust. For vaporization to be effective, the liquid sheet must be atomized for the liquid film to form droplets and the effectiveness of this atomization process depends on the type of injector used. In the LPP concept, when vaporization is complete, the fuel and the oxidizer must be thoroughly mixed before entering the combustion chamber [6, 7]. Not setting the right droplet sizes, for instance, can lead the formation of hot spots if the droplets size are over-predicted, which can lead to liquid droplets entering the combustion chamber. Flashback will occur if the droplets sizes are too small, leading to overheating of the droplets inside the mixing chamber. Thus, one of the most challenging aspects of modeling liquid fuel combustion is the atomization process.

In addition to the above, diesel, like most liquid fuels, is multi-component and very little is known about modeling such fuels [6]. Diesel is made of large proportions of different components with each containing carbon atoms ranging from 9 to 23. Of these components, gas-oil ($C_{16}H_{29(l)}$) makes up the largest percentage by mass [6]. To simplify the modeling, gas-oil is used as a surrogate for diesel in all the simulations in this work.

The main objective of this paper is to report the successful determination of the atomization model for the Schlick injector based on measurement data. CFD simulations of the cold and hot flows are performed and the results obtained are compared with those obtained when the uniform droplet size distribution was used. The paper begins with a description of the experimental setup of the matrix burner followed by the presentation of the CFD model setup. This is followed by the detailed discussion of the atomization model after which the CFD results and discussions are presented. The paper is ended by presenting the conclusions and the future outlook.

EXPERIMENTAL SETUP OF MATRIX BURNER

A sketch of the experimental setup of the test rig is shown in Fig. 1. The test rig was designed to study self-excited thermoacoustic instabilities.

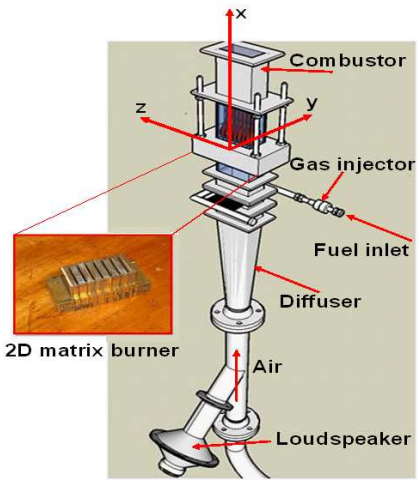

FIGURE 1. SKETCH OF THE TEST RIG USED IN MEASUREMENTS.

The test rig consists of air and fuel supply systems, an ignition or pilot flame, and a premixing chamber. Once ignition is completed, the pilot flame is switched off. Upstream propagation of the flame is prevented by a 2D matrix element, which has seven slots, each measuring 2.5mm x 40mm in cross-section and 50mm in height as shown in Fig. 1. The air inlet pipe is a DN 50 pipe with an inner diameter of 42mm. The test facility is equipped with sensors and instruments for measuring the air and the fuel mass flow rates, pressure, temperature, heat release and emissions.

The combustion air is supplied by a screw compressor at constant pressure. The air flow rate is determined separately and can be adjusted. It is measured through a laminar mass flow meter within an accuracy of $\pm 5\%$. It enters the test rig at the air inlet (see Fig. 2) and a honey comb is placed downstream to streamline the air flow. The air leaving the honey comb flows through a diffuser that lowers the air velocity and decreases the pressure loss across the burner. The fuel, which is diesel in this case, is injected from the sidewall of the mixing tube using six pressure swirl atomizers. The injected fuel interacts with the fast moving air stream and the liquid droplets are heated up in the process to their boiling point temperature of 512K, after which they vaporized. The vaporized fuel then mixes with the air before entering the combustion chamber. Details of the geometry of the injector as well as the description of the atomization process are discussed under atomization model. The combustor has a cross section of 92mm x 46mm and add-ons that makes it possible to use variable combustor lengths of 200mm, 400mm, 600mm, 800mm and 1000mm. The length used in this work is 1000mm. The outlet of the combustor is connected to a flexible tube of length 6m that exhausts the combustion products to the atmosphere. The exhaust gas temperature is measured using a PtRh-Pt thermocouple. The combustion chamber is surrounded with mineral wool to reduce thermal losses because it was not air or water cooled. The test rig can be operated at equivalence ratios between 0.59 and 1.6. Detailed description of the experimental setup can be seen in [2, 5, 6].

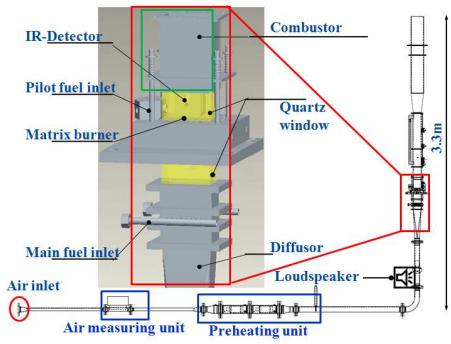

FIGURE 2. SCHEMATIC OF THE MATRIX BURNER.

CFD MODEL SETUP

Model abstraction is critical in CFD simulation because of the need to simplify of the analysis, while at the same time making sure that the physics of the problem is captured. To limit the size of the computational grid, the ducts at the inlet and outlet are not included in the computational mesh. The approach in this case is to determine their impedances and superimposed them on the CFD simulation as discussed in details in [5].

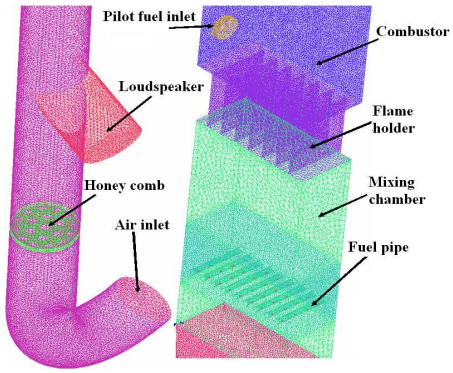

FIGURE 3. CFD SURFACE MESH OF THE TEST RIG.

The mesh of the CFD model simulated is shown in Fig. 3. The CAD drawing was done using Pro/Engineer and the mesh was generated using ICEM CFD. The mesh is unstructured and tetrahedral. For the sake of clarity, the surface mesh, with no volume is shown and it has a size of 0.77 million cells. A line diagram of the CFD model is given and discussed in [2].

Solver and Boundary Conditions

The Fluent 6.3 pressure coupled solver was used. For discretizing the governing equations the QUICK scheme was used. Time matching was done implicitly using a second order scheme. For turbulence modeling, the $k-\varepsilon$ realizable model was used. The reason for using this model is given in [6]. The CFD simulations are done using four parallel processes, each using a total of two processors on a Linux cluster at the RWTH Aachen University high performance computing center. The CPU is an AMD Opteron 885 that has a 2.6 GHz (dualcore) processor with a memory of 32 GByte per node.

The CFD boundaries used for the simulations are as follows: the air inlet is given a velocity inlet boundary and the combustor outlet is treated as a pressure outlet. The rest of the surfaces are treated as walls with no slip and adiabatic conditions. Liquid fuel is admitted using the Discrete Phase Model (DPM) in Fluent with the injectors introduced using six injection files that are created by a Fortran subroutine. The files are created using measurement data reported in details under atomization model. The

operating pressure is atmospheric and gravity is imposed in the negative x-direction along the combustor axis because the test rig is vertical. By doing this, the effect of gravity and buoyancy, though not large, on the combustion process are accounted for in the CFD simulations. The walls are given trap boundary and in this case when the droplets collide with the walls their mass instantaneously passes into the vapor phase and enters the cell adjacent to the boundary. The conservation of mass and energy principles are obeyed since no energy is taken from the computational domain for vaporizing the droplets that hit the walls.

Combustion Model

The species transport equation or the balance equations for the mass fraction of species i can be written as:

$$\frac{\partial}{\partial t}(\rho Y_i) + \nabla \cdot (\rho \mathbf{u} Y_i) = -\nabla \cdot \mathbf{J_i} + \omega_i, \tag{1}$$

where $i = 1, 2, 3, ...n$. The left hand side terms represents the local rate of change and convection. The first term on the right hand side is the diffusion flux denoted by $\mathbf{J_i}$ and given by $\mathbf{J}_i = -\rho \mathbf{D}_i \nabla Y_i$, where $\mathbf{D}_i$ is the binary diffusion coefficient or mass diffusivity of species i. The last term is the chemical source term, which is unclosed. It is closed in this work by using the combined finite rate/eddy dissipation model [8]. This model determines the Arrhenius rate and the eddy dissipation rate and picks the smaller of the two as the net rate of reaction. The assumption of a one step irreversible reaction is used. It is of the form:

$$\nu'_F F + \nu'_O O \rightarrow \nu'' P, \tag{2}$$

where F is the fuel and O is the oxidizer. In the eddy dissipation model, the rate of the reaction is given by the net rate of production of species i due to reaction r, denoted by $\omega_{i,r}$ and given by $\omega_{i,r} = min(\omega_{i,r1}, \omega_{i,r2})$, where

$$\omega_{i,r1} = \nu'_{i,r} W_i A \bar{\rho} \frac{\varepsilon}{k} \min_R \frac{Y_R}{\nu'_{R,r} W_R}, \tag{3}$$

and

$$\omega_{i,r2} = \nu' W_i A B \bar{\rho} \frac{\varepsilon}{k} \frac{\sum_P Y_P}{\sum_i^N \nu'' W_i}. \tag{4}$$

Y_P is the mass fraction of any product species P; Y_R is the mass fraction of a particular reactant, R; ε is the turbulent dissipation rate; k is the turbulent kinetic energy; A and B are empirical constants equal to 4.0 and 0.5 respectively.

In the finite rate chemistry model, the rate for the second order reaction used is given by:

$$\omega = B \bar{\rho} \frac{Y_F}{W_F} \bar{\rho} \frac{Y_{O2}}{W_{O2}} \exp\left(\frac{-E}{RT}\right). \tag{5}$$

If we assume that the reaction is first order with respect to the fuel, then the rate expression becomes

$$\omega = B' \bar{\rho} \frac{Y_F}{W_F} \exp\left(\frac{-E}{RT}\right), \tag{6}$$

where B', the frequency factor, is related to B in Eqn. (5) by $B' = B \bar{\rho} \frac{Y_{O2}}{W_{O2}}$. B' has units of $1/\mathrm{s}$ whereas in Eqn. (5), B has units of $\mathrm{m}^3/(\mathrm{kmol\ s})$.

Liquid Fuel Vaporization and Thermophysical Properties

Vaporization is the rate at which liquid mass (or droplet radius) is decreasing due to phase transition. For evaporating droplet, the cooling of the droplet due to the energy loss resulting from the change of state (from liquid to gas) of some of its mass has to be accounted for. This is given by the droplet temperature evolution as [9]:

$$\frac{\mathrm{d}T_d}{\mathrm{d}t} = \frac{T_s - T_d}{\tau_{d,T}} + \frac{L(T_d)}{m_p C_p} \dot{m}_p, \tag{7}$$

where $L(T_d)$ is the latent heat of vaporization of the droplet at temperature T_d, $\dot{m}_p = \frac{\mathrm{d}m_p}{\mathrm{d}t}$ is the vaporization rate and $\tau_{d,T}$ is the particle thermal relaxation time.

It is very important to be able to accurately predict the rate of droplet vaporization. Several models for droplet vaporization exist. Prominent amongst them is the d-squared (d^2) law [9]. In this model, the diameter d at time t is related to the initial diameter d_0 by the vaporization constant k. The model equation is therefore:

$$d^2 = d_0^2 - kt. \tag{8}$$

This model is used for a single droplet vaporization. The vaporization model used in this work is developed by [9] and implement in the DPM in Fluent. This model is simple and it assumes

that droplets are spherical and that the temperature throughout the droplets is the same. Droplets are uniformly heated from their evaporation temperature, which is taken as 300K to their vaporization or boiling temperature, which is taken to be 512K for gas-oil. At the boiling point the temperature throughout the droplets is the same during phase change from liquid to vapor and this is referred to as the wet-bulb temperature.

The thermophysical properties play a crucial role in the simulation of liquid fuels. Properties like the boiling point depend on the pressure and must be accurately determined. The C_p values must also be determined as a function of temperature. In the simulations carried out in this work, the operating pressure was 1bar and these properties are determined at this pressure. Details description of how the C_p, boiling point, etc, were determined and their effect on the combustion simulation are discussed in details in [6].

Stochastic Particle Technique

A very efficient and accurate method for solving for the spray dynamics is based on the Monte Carlo and discrete particle methods [9]. In this method, the continuous distribution f is approximated by a discrete distribution f' given by:

$$f' = \sum_{p=1}^{n_p} n_p \delta(\mathbf{x}-\mathbf{x}_p)\delta(\mathbf{v}-\mathbf{v}_p)\delta(r-r_p)\delta(T_d-T_{d_p})\delta(y-y_p)\delta(\dot{y}-\dot{y_p}). \tag{9}$$

Each particle p is composed of a number of droplets n_p having equal location $\mathbf{x}_p$, velocity $\mathbf{v}_p$, size r_p, temperature T_{d_p}, and oscillation parameters y_p and $\dot{y_p}$. The particle and droplet trajectories coincide (for example, $\frac{\mathrm{d}\mathbf{x}_p}{\mathrm{d}t} = \mathbf{v}_p$ and $\frac{\mathrm{d}\mathbf{v}_p}{\mathrm{d}t} = \mathbf{F}_p$) and the particles exchange mass, momentum, and energy with the gas in the computational cells in which they are located. This method is Monte Carlo in the sense that sampling is made randomly from assumed probability distributions, in this case, the random walk model, that govern droplet properties at injection and droplet behavior subsequent to injection. The error associated with this method depends on the number of droplets. It can be shown that in general, error $\sim 1/\sqrt{n_p}$. But mostly a trade-off is needed because using too many droplets leads to an increase in the computational cost.

ATOMIZATION MODEL

The process of oil combustion modeling can be divided into the following: atomization, evaporation, mixing and combustion. The flow consists of two phases, liquid fuel and air. In the modeling of most two phase flows, the Eulerian-Lagrangian approach is used. The continuous phase (gaseous phase) is modeled using the Eulerian framework while the discrete or liquid phase is modeled using the Lagrangian framework. The main drawback is the fact that the model equations associated with each method have to be discretized using different numerical schemes. The Lagrangian method also needs an optimum number of computational particles for proper statistics and turbulence representation. This method is computationally expensive. Another method assumes that the flow is locally homogeneous and so it solves the same sets of equations (continuity, momentum, energy, species transport and turbulent transport equations) for each phase. Here, the same discretization scheme is used but there is an increased in the number of equations that have to be solved. The latter approach falls under locally homogeneous flow (LHF) model while the former falls under separated flow (SF) model. For the LHF model, the gas and liquid phases are assumed to be in dynamic equilibrium (that is, at each point in the flow both phases have the same velocity and temperature and are in phase equilibrium). This is a limiting case and holds true only for sprays consisting of infinitely small drops. In the case of the SF model, finite rates of transport between the two phases are considered. This approach is commonplace in modeling most two phase flows because of the enormous advantage it offers when dealing with complex spray discretization and flow phenomena such as secondary breakup or droplet-wall interaction. Details on the available approaches available for modeling liquid fuels for applications in both diesel engines and gas turbines are discussed in [9, 10, 11, 12, 13, 14, 15, 16, 17].

The modeling approach used in this work is the Lagrangian-Eulerian method that is implemented in the Discrete Phase Model (DPM) in Fluent. One short coming of the Lagrangian approach of the particle phase is that it neglects particle-particle interaction. The "parcel" model, adopted here, only partially addresses this short-coming and thus is appropriate for dilute spray applications, unlike the spray from the Schlick injector, which is dense. One example of this short coming is in the simulation of hot flow where the drops are assumed to evaporate on the same time scale as the transport. However, this method has been used at this stage to yield only representative results.

In general, in the simulation of liquid fuel, the fuel is first atomized followed by vaporization, mixing and combustion. This is the so-called lean-premixed prevaporized (LPP) combustion concept that is being adopted in the design of new gas turbines. Of these, the most critical is the atomization process. In this process, the initial conditions of the droplets like the velocities, temperature and droplet sizes must be specified. For example, underestimating the velocities of the droplets can lead to staggering of the droplets in the computational domain. To solve such a problem, the nozzle diameter can be reduced. If the droplet velocities are too large, the residence time is reduced and it could lead to droplets entering the combustion chamber and this could lead to the production of harmful gases like NOx and sooth [18]. Even though standard models exist for hollow cone nozzles in the Fluent solver, they cannot be taken to universally work for every nozzle. Great care must therefore be taken when they are

used.

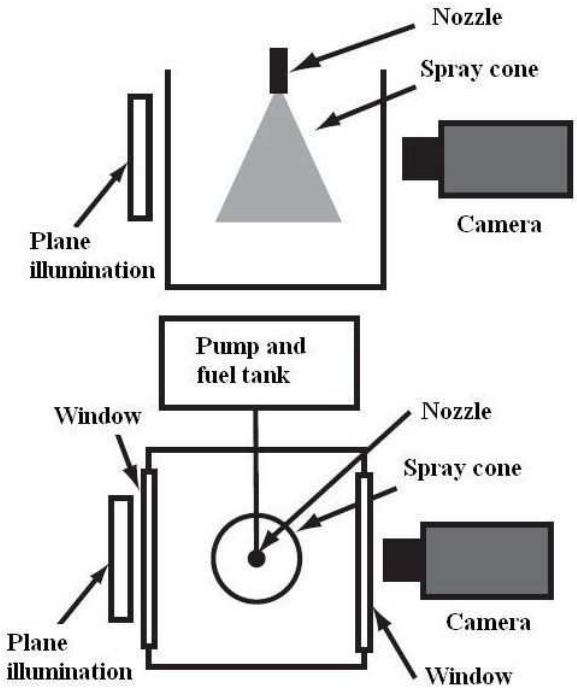

FIGURE 4. SCHEMATIC ILLUSTRATION OF THE TEST RIG USED IN THE SPRAY VISUALIZATION (TOP: SIDE VIEW, BOTTOM: TOP VIEW) TAKEN FROM [19].

To overcome this problem the atomization model of the Schlick pressure swirl atomizer used in this work is developed from measurement data. The measurement was done at the Institute of Heat and Mass transfer at the RWTH Aachen University within the collaborative research project SFB 686 [19]. As measurement techniques, visualization and Phase Doppler Anemometry (PDA) were used. In Fig. 4, the experimental setup of the visualization test rig used in the injector measurements is shown. The data analyzed in this work were measured in two planes located 5mm and 50mm downstream of the nozzle. To determine the droplet size distribution only measurements done 5mm from the nozzle are considered. It was difficult to measure at a position less than 5mm from the nozzle. The atomization model developed is therefore referred to as prompt atomization since in this case, primary breakup of droplets is not considered. This is only true if the time scale of the primary breakup, when compared to the total fuel residence time is smaller. Primary breakup therefore finishes very close to the nozzle exit. Figure 5 shows an example of the spray obtained from measurements for the 25bar injection pressure case. In the following, the determination of the atomization model from measurements is presented followed by the CFD results and discussions and finally the conclusions.

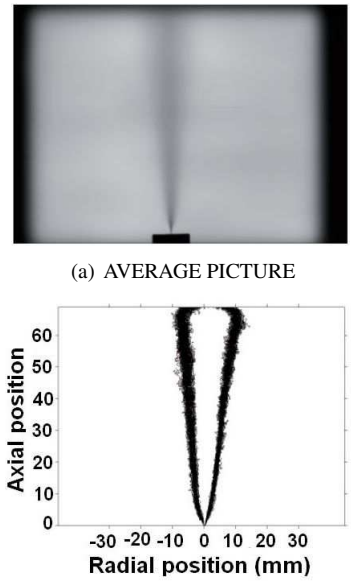

(a) AVERAGE PICTURE

(b) CONTOUR

FIGURE 5. AVERAGED PICTURE (TOP) AND CONTOUR PLOT (BOTTOM) FOR Δp=25BAR TAKEN FROM [19].

Determination of the Atomization Model from Measurements

A CAD drawing of the setup used with the liquid fuel nozzles arranged at the sidewalls of the mixing chamber is shown in Fig. 6(a). The sketch is cut in the middle to show the injectors. In total, six injectors are arranged on the sidewalls of the mixing chamber.

The picture of the Schlick injector that is modeled in this work is shown in Fig. 6(b). The nozzle used for this work is a hollow cone pressure swirl atomizer. It is of the Schlick series 121 - 123 Kreisl nozzle and the model is 121 V S51. The internal design of the nozzle allows for swirling of the liquid before it is injected. The swirl factor is defined mathematically as:

$$sf = \frac{2G_m}{D_{sw}G_t}, \tag{10}$$

where G_m is the axial flux angular momentum, G_t is the axial trust and D_{sw} is the swirl diameter. Two nozzle diameters are considered. In one case, a nozzle diameter of 0.1 mm is used and in the other, the diameter used is 0.2mm. The spray cone

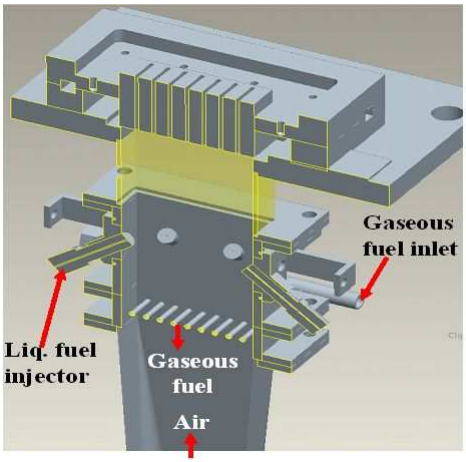

(a) CAD DRAWING, WITH FOUR SCHLICK INJECTORS

(b) PICTURE, SCHLICK INJECTOR

FIGURE 6. CAD DRAWING AND PICTURE OF THE SCHLICK INJECTOR.

angle lies between 16°-18° for the 0.1mm nozzle diameter case and 60° for the 0.2mm diameter case. The latter is an analytical atomization model used for doing preliminary parametric studies using CFD while the former is based on measurement data. For example, using parametric studies with the help of CFD, it was found that the optimum arrangement of the injectors should be from the sidewalls of the mixing tube. The number of injectors that resulted in the best mixing between the fuel and oxidizer are 6. Detailed description of the preliminary design work that was done is reported in [6].

The mass flow rates of the fuel are measured for various injection pressures. The injection pressures considered in the measurements are 15bar, 20bar, 25bar and 30bar. Injection pressures below 15bar were also considered because the spray obtained in these cases were not well defined. The mass flow rates of the injector is determined at the Institute for Power Plant Technology, Steam and Gas Turbines at the RWTH Aachen University and this is compared with the mass flow rates determined using the data sheet from Schlick. The mass flow rates determined are shown in Tab. 1. The difference between them is little, confirming that they are accurately determined. Using the mass flow rates determined, the nozzle discharge coefficients are determined for each injection pressure using:

$$\dot{m} = \rho \frac{\pi D^2}{4} \alpha_D \sqrt{\frac{2\Delta p}{\rho}} \tag{11}$$

and also reported in Tab. 1. In Eqn. (11), ρ is the density of gas-oil, which is 820 kg/m^3, D is the nozzle diameter = 0.1 x 10^{-3}m, Δp is the pressure drop across the nozzle in N/m^2 and α_D is the discharge coefficient.

TABLE 1. MASS FLOW RATES AND DISCHARGE COEFFICIENTS OF SCHLICK NOZZLE.

Δp (bar)	$\dot{m}$(kg/s) Measurements	$\dot{m}$(kg/s) Schlick data sheet	α_D[-]
20	5.47 x 10^{-4}	5.47 x 10^{-4}	1.2
25	6.15 x 10^{-4}	6.12 x 10^{-4}	1.2
30	6.49 x 10^{-4}	6.49 x 10^{-4}	1.2

Using the mass flow rates above and the continuity equation, which is given by:

$$\dot{m} = \rho \frac{\pi D^2}{4} u_{mod}, \tag{12}$$

the injection velocity, u_{mod}, is determined. In the case of multiple injectors like we have, the mass flow rate per injector must be used in the continuity equation. For the case of 25bar injection pressure, we will get an injection velocity of 15.88m/s for the six injectors considered, if the average of the mass flow rates shown in Tab. 1 is used. The component of the velocities in the x, y and z direction are then determined using the sketch in Fig. 7. i_x, i_y and i_z denote the unit vectors of the injector along the x, y and z axes and they are given by $i_x = cos\gamma$, $i_y = sin\gamma sin\alpha$ and $i_z = sin\gamma cos\alpha$, where γ is the half-spray cone angle and α is the angle the nozzle axis makes with the horizontal.
The corresponding three velocity components according to the sketch in Fig. 7 can be written as:

$$\begin{aligned} u_x &= i_x u_{mod} \\ u_y &= -u_{mod}(i_z cos\alpha + i_y sin\alpha) \\ u_z &= u_{mod}(i_z sin\alpha - i_y cos\alpha). \end{aligned} \tag{13}$$

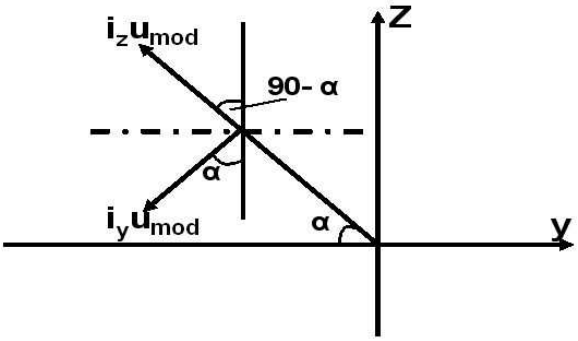

FIGURE 7. UNIT VECTORS OF THE NOZZLE ARRANGED ON THE SIDEWALL OF THE MIXING CHAMBER.

Droplet Size Distribution The droplet size distribution is also critical in determining the atomization model. Many factors affect the droplet size distribution. Among them, the type (nozzle design) and diameter of the nozzle play a major role. The length of the injector also affects the atomization process. The histogram of the droplets measured in the plane 5mm from the nozzle are shown in Figs. 8(a) and 8(b) respectively for the 20bar and 25bar injection pressure cases. In the plots shown, only droplets upto 100μm are taken into consideration. The total number of droplets in the measurements are 50 000. In another case not shown in the plot, but for which the droplet size distribution is presented, diameters of droplets upto 50 μm are considered. In the former, only 1% of droplets had diameters greater than 100μm while in the latter, only 4% of droplets had diameters greater than 50μm. Even though bigger droplets contribute more to the volume of the spray, the number of droplets with size greater than 50μm and 100μm are very small. Besides, the nozzle diameter of 0.1mm makes it unrealistic to have droplets of size larger than 50μm or 100μm.

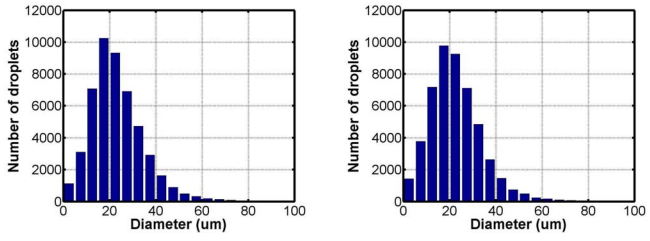

(a) Δp=20bar (b) Δp=25bar

FIGURE 8. HISTOGRAM SHOWING DISTRIBUTION OF DROPLET IN PLANE 5MM AWAY FROM THE NOZZLE.

Typical droplet size distribution include the uniform distribution, Gaussian distribution, root normal distribution and the Rosin-Rammler distribution [18]. For many applications the droplet size distribution are mostly root normal or Rosin-Rammler, although in simple cases, the uniform distribution can be used (for example, when the spread parameter in the Rosin-Rammler distribution, δ is infinitely large).

The Root-normal distribution is given by:

$$f(d) = \frac{x}{2\sigma_s d\sqrt{2\pi}} \exp\left[-0.5\left(\frac{x-\mu}{\sigma_s}\right)^2\right], \qquad (14)$$

where $x = \sqrt{\frac{d}{MMD}}$, d is the droplet diameter in μm, MMD is the mean mass diameter in μm, μ is the mean and σ_s is the standard deviation of the distribution. μ and σ_s are determined experimentally. This is a single parameter distribution as can be seen from Eqn. (14). To determine whether the distribution of the droplet from the Schlick nozzle is according to this distribution, the Simmons' universal root normal distribution rule is used [20]. It states that for a root normal distribution the ratio $MMD/SMD = 1.2$, where $MMD = \left(\frac{\sum nd^3}{\sum n}\right)^{0.33}$ and $SMD = \frac{\sum nd^3}{\sum nd^2}$, with n being the number of droplets with diameter d. This ratio was determined for the 25bar case and plotted as shown in Fig. 9 for the range of droplets upto 50 μm. From this plot, we can conclude that the distribution is not root normal since $MMD/SMD \neq 1.2$.

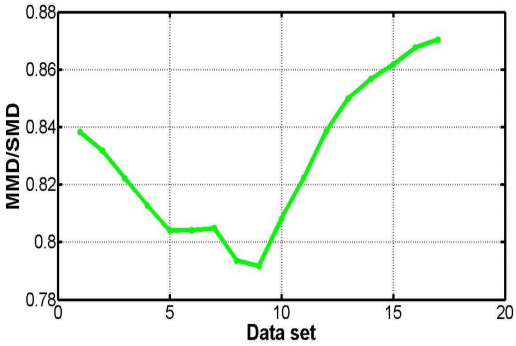

FIGURE 9. RATIO OF MMD TO SMD FOR THE Δp=25BAR CASE AND FOR DROPLETS SIZE UPTO 50μm.

The MMD is defined in this case as drop diameter below or above which lie 50% of the mass of the drops while the SMD is defined as the diameter of a drop having the same volume/surface ratio as the entire spray [18]. Other mathematical definition of mean size are: (a) linear mean diameter, (d_1), which is given by $d_1 = \frac{\sum nd}{\sum n}$;

(b) area length (d_0), which is defined as the diameter of a drop having the same surface/diameter ratio as the entire spray and given mathematically as $d_0 = \frac{\sum nd^2}{\sum nd}$; (c) area diameter ($d_2$) and this is the diameter of a drop whose surface area is equal to the mean surface area of all the drops in the spray and is given by $d_2 = \left(\frac{\sum nd^2}{\sum n}\right)^{0.5}$.
Three of these parameters, namely, the SMD, MMD and the linear mean diameter, d_1, are determined for the various data set from measurements for droplet diameters of upto 50 μm and plotted in Fig. 10.

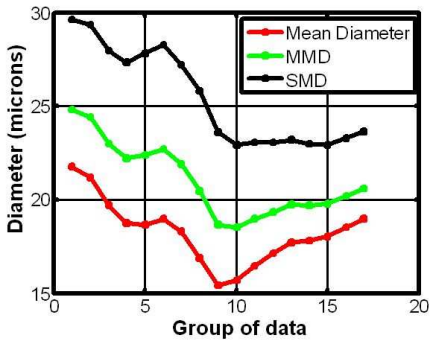

FIGURE 10. PLOT OF THREE MEASURES OF DROPLET DIAMETERS TAKEN FROM MEASUREMENTS WITH THE SCHLICK INJECTOR, Δp=25BAR.

The next distribution that is considered is the Rosin-Rammler distribution. It is the most widely used expression for droplet size distribution. It is a two parameter distribution that was originally developed for powders by Rosin and Rammler. Mathematically, it can be written as:

$$\nu = F(d) = 1 - \exp\left[-\left(\frac{d}{d_m}\right)^{\delta}\right], \qquad (15)$$

where $F(d)$ is the cumulative density function (cdf) or the fraction of the total volume contained in drops of diameter less than d, d_m is the Rosin-Rammler mean diameter of the droplets and δ is a constant that is referred to as the Rosin-Rammler skewness parameter that determines the spread of the drop sizes. The higher the value of δ, the more uniform the spray. For $\delta = \infty$, the drops are of the same sizes. For most sprays, the value of δ is between 2 and 4 [18, 21].

The droplet size distribution or the probability density function (pdf), denoted as $f(d)$, is obtained by taking the derivative of the cumulative density function. That is, $f(d) = F'(d)$, where $F'(d)$ denotes the derivative of $F(d)$ with respect to d, the diameter of the droplets. Applying this to Eqn. (15), we get:

$$f(d) = -\frac{\delta}{d}\left(\frac{d}{d_m}\right)^{\delta} \exp\left[-\left(\frac{d}{d_m}\right)^{\delta}\right]. \qquad (16)$$

The parameters d_m and δ are determined from measurement data reported in [19]. Two cases are considered. In the first case, only droplets of diameter less than 50 μm are considered. In the other case, droplets of diameter less than 100 μm are considered. The analysis was done for the 25bar injection pressure case. To determine the constants in the cdf, least square regression analysis is used. A graph of $ln(1-\nu)$ is plotted against d, the droplets diameter from the measurements. These curves are fitted as shown in Figs. 11(a) and 11(b). The small cone angle is an indication that the spray is very narrow as it was observed in the measurements. This is an indication of an increased number density of particles. From the plots in Figs. 11(a) and 11(b), the maximum experimentally determined volume fraction of the spray 5mm from the nozzle exit is 0.998.

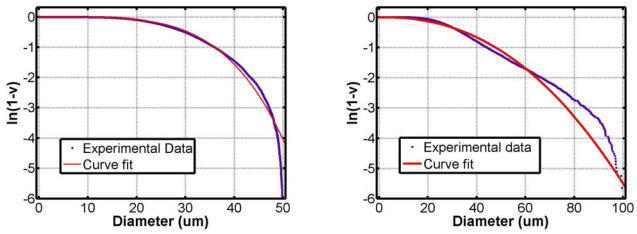

(a) DROPLETS SIZE UPTO 50μm (b) DROPLETS SIZE UPTO 100μm

FIGURE 11. CURVE FITTING USING REGRESSION ANALYSIS Δp=25BAR.

The goodness of fit value, R^2 is 0.93 for the case of droplet diameters upto 50μm and 0.87 for the case of droplet diameters upto 100μm indicating that we have a better fit for the former than for the latter. The constants d_m and δ are determined to be 35.9μm and 4.244 respectively for the case of droplets with diameter upto 50μm and 47.62μm and 2.299 respectively for the case of droplets with diameter upto 100μm. The equation of the cdf for droplets upto 50μm case can be written as:

$$F(d) = 1 - \exp\left[-\left(\frac{d}{35.9}\right)^{4.244}\right], \qquad (17)$$

and that for droplets of diameter upto 100μm can be written as:

$$F(d) = 1 - \exp\left[-\left(\frac{d}{47.6}\right)^{2.299}\right]. \qquad (18)$$

In Figs. 12(a) and 12(b), curves of the cumulative density functions together with their experimentally determined counterparts are plotted. The two curves are closer in the case for diameters upto 50 μm than in the case for droplets with size upto 100 μm.

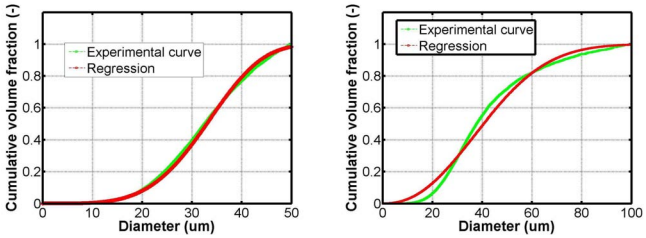

(a) DROPLETS SIZE UPTO 50μm (b) DROPLETS SIZE UPTO 100μm

FIGURE 12. CUMULATIVE VOLUME FRACTION CURVES, Δp=25BAR.

The pdf of the case with droplets upto 50 μm can be written as:

$$f(d) = -\frac{4.244}{d}\left(\frac{d}{35.9}\right)^{4.244} \exp\left[-\left(\frac{d}{35.9}\right)^{4.244}\right], \qquad (19)$$

while that for droplets size upto 100 μm is given by:

$$f(d) = -\frac{2.299}{d}\left(\frac{d}{47.6}\right)^{2.299} \exp\left[-\left(\frac{d}{47.6}\right)^{2.299}\right] \qquad (20)$$

The corresponding plot of the distributions for both cases are shown in Figs. 13(a) and 13(b). These distributions are implemented in a Fortran subroutine to generate the injection files that are hooked to the Fluent solver.

The volume fraction distribution from the Fortran subroutine that is used to generate the injection files together with the cumulative mass flow rate and the distribution of the mass flow are shown in Fig. 14 for an injection pressure of 25bar. In this case, the total mass flow rate per injector is 1.02 x 10^{-4} kg/s as can be seen from the cumulative mass distribution curve.

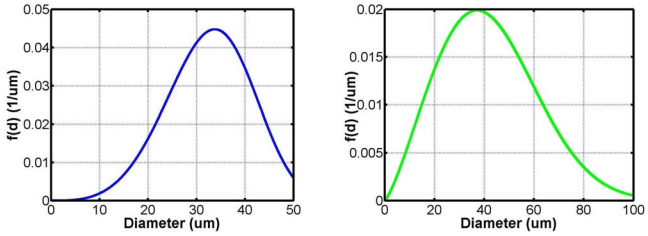

(a) DROPLETS SIZE UPTO 50μm (b) DROPLETS SIZE UPTO 100μm

FIGURE 13. DROPLET SIZE DISTRIBUTIONS, Δp=25BAR.

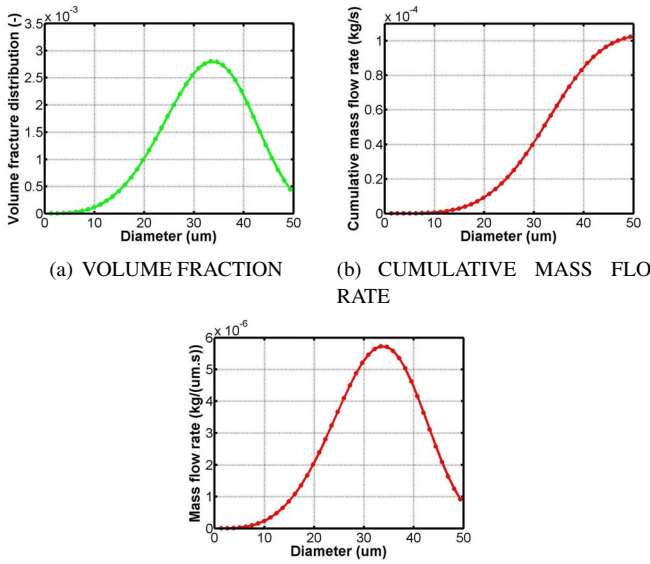

(a) VOLUME FRACTION (b) CUMULATIVE MASS FLOW RATE

(c) PDF OF MASS FLOW RATE

FIGURE 14. VOLUME FRACTION & MASS FLOW DISTRIBUTION OF DROPLET FROM THE FORTRAN SUBROUTINE FOR DROPLETS SIZE UPTO 50μm.

RESULTS AND DISCUSSIONS

Cold Flow

The cold flow simulation based on the Rosin-Rammler droplets size distribution implemented in the Fortran subroutine is presented and discussed. Detailed description of the atomization model setup is reported in the section above. The cold flow results for which the droplets size distribution is uniform are reported in [6]. The case reported here has a ϕ value of 0.59 and an air mass flow rate of 15.016 g/s. The air is preheated to a temperature of 425^{o}C, which is the typical compressor outlet temperature in gas turbines. The liquid fuel simulated is gas-oil ($C_{16}H_{29}$). Three cases are considered, namely: spray cone angles 17^o, 40^o and 60^o. The first case corresponds to the average spray cone angle of the Schlick injector as recorded from measurements [19]. The axial distance of the nozzle from the com-

bustor inlet is kept fixed at 188mm. The unmixedness parameter, β, is determined in five planes in the mixing chamber and plotted in Fig. 15. The case with the best mixing field is the cone angle 17^o case as expected, because this is the cone angle of the injector that was determined from measurements. The case with the second best mixing field is the spray cone angle 40^o case.

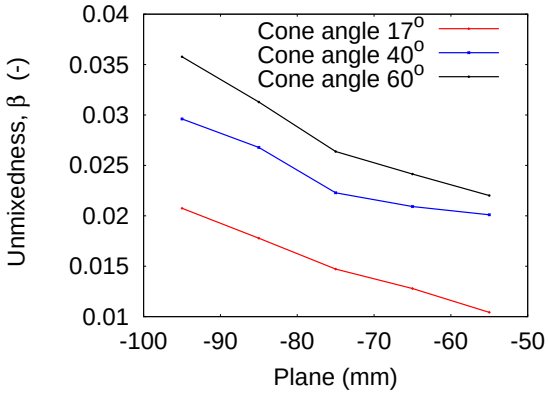

FIGURE 15. UNMIXEDNESS PARAMETER IN FIVE PLANES INSIDE THE MIXING CHAMBER.

The unmixedness parameter shown in Fig. 15 is given by:

$$\beta = \frac{\Sigma_{i=1}^{N} Y_{Fi}^2 - N(\bar{Y}_F)^2}{N\bar{Y}_F(1-\bar{Y}_F)}, \tag{21}$$

where N is the number of vertices in the plane. The numerator in Eqn. (21) is the variance of the fuel mass fraction, which can be written as $\sigma^2 = \frac{\Sigma_i (Y_F - \bar{Y}_F)^2}{N}$.

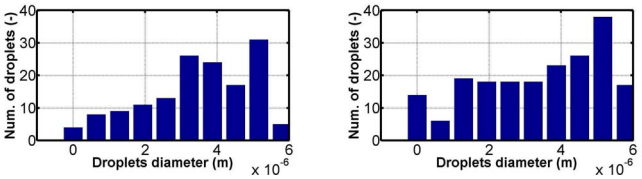

(a) AXIAL DIS. -188mm, PLANE x=-55mm (b) AXIAL DIS. -188mm, PLANE x=-65mm

FIGURE 16. HISTOGRAM OF DROPLETS IN PLANES IN THE MIXING CHAMBER, ϕ=0.59, $\dot{m}_{air} = 15.016$g/s.

Observation of the histogram of droplets in two planes (namely, planes x=-55mm and x=-65mm) inside the mixing chamber shows that liquid droplets are present in these planes. Mixing of the fuel and the oxidizer is therefore less optimum in these planes. It is also possible that in such a situation, liquid droplets can enter the slots of the flame holder and the combustion chamber. This obviously leads to the generation of hot spots in the combustion zone with an increase in sooth generation. One solution to this problem, apart from reducing the size of the droplets, is to increase the residence time of the fuel in the mixing chamber. This can be achieved by increasing the axial distance of the nozzle from the combustor inlet. Three distances for the cone angle 17^o case are investigated. The baseline case is 188mm and the other two cases considered are 218mm and 228mm. In each case, droplets are monitored in the planes x=-55mm and x=-65mm. For the case where the axial distance is 188mm large number of droplets are visible in both planes. In the case of the 218mm axial distance, many droplets are in the x=-65mm plane and small number of droplets are visible in the x=-55mm plane. The histograms of droplet size in two planes in the baseline case are shown in Fig. 16. For the case where the axial distance is 228mm, small number of droplets are reported in the plane x=-65mm and no droplets appear in the plane x=-55mm, suggesting that this could be the ideal location for the nozzles of the Schlick injectors. The mean and standard deviation of the droplets in each case are determined. For the axial distance of 188mm case, the mean and standard deviation in the plane x=-55mm are $3.46707\mu m$ and $1.4756\mu m$ respectively, while the mean and standard deviation in the plane x=-65mm case are $3.3884\mu m$ and $1.7243\mu m$ respectively. For the axial distance of 218mm, the mean and standard deviation in the plane x=-55mm are $3.0088\mu m$ and $0.0737\mu m$ respectively, while the mean and standard deviation in the plane x=-65mm are $2.8787\mu m$ and $1.6863\mu m$ respectively. For the 228mm axial distance case, the mean and standard deviation in the plane x=-55mm are zero, while the mean and standard deviation in the plane x=-65mm are $2.3075\mu m$ and $2.4743\mu m$ respectively.

A User Defined Function (UDF) that determines the Sauter mean diameter or SMD (D_{32}) is used to confirm the results reported above. In this case, the SMD is determined in the transverse y direction along the lines z=0 and x=-65mm and plotted as shown in Fig. 17. From the plots, the SMD shows some degree of symmetry about the middle axis and the values of the SMD are decreasing with increasing axial distance of the nozzles. In the case where the axial distance of the nozzles is 228mm, plotting the SMD in the transverse y direction (along the width of the mixing chamber) at x=-55 and along the y-axis (z=0) gave a value of zero, thus confirming the earlier results reported.

Hot Flow

Comparison is done between the steady flames obtained using the uniform distribution and the Rosin-Rammler distribution. In the case of the former, the Sauter mean diameter used is 30

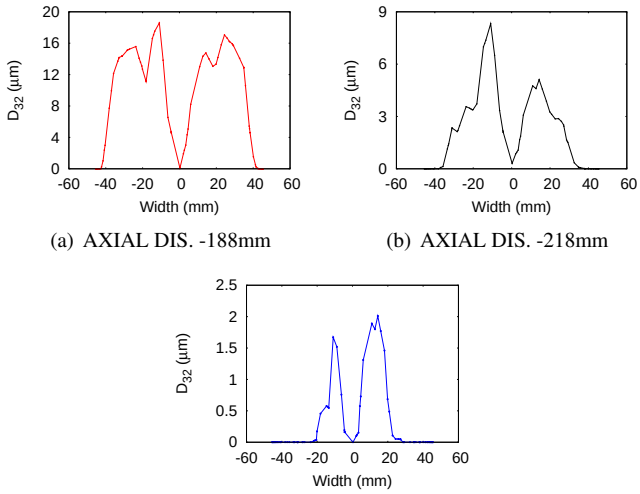

(a) AXIAL DIS. -188mm

(b) AXIAL DIS. -218mm

(c) AXIAL DIS. -228mm

FIGURE 17. SMD ALONG THE WIDTH OF THE MIXING CHAMBER, DISTANCE FROM THE COMBUSTOR INLET = 65mm, ϕ=0.59, $\dot{m}_{air} = 15.016$g/s.

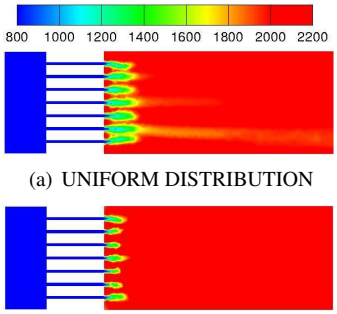

(a) UNIFORM DISTRIBUTION

(b) ROSIN-RAMMLER DISTRIBUTION FOR DROPLETS UPTO 50 μm

FIGURE 18. STEADY LIQUID FLAME TEMPERATURE (K), PLANE Z=0, ϕ=0.59 FOR TWO DIFFERENT DROPLET SIZE DISTRIBUTIONS.

μm and the spray cone angle is 60^o while the air mass flow rate is 29.81 g/s (See [6] for more information). In the latter case, the Rosin-Rammler distribution is used. The Rosin-Rammler mean diameter is 35.9 μm and the air mass flow rate is 15.016 g/s. In both cases, the air is preheated to 425^oC and the equivalence ratio is 0.59. The axial distance of the nozzle from the combustion chamber inlet is 188mm in both cases. The steady flames obtained in both cases are shown in Fig. 18. The flame length for the uniform distribution case is slightly longer than that obtained using the Rosin-Rammler distribution. This could be due the differences in the inlet velocities. The temperatures obtained using both distributions are different with the latter looking more homogeneous than the former. Therefore, using a uniform distribution to represent the Schlick hollow cone nozzle can lead to differences in the flame behavior obtained from measurements and that obtained from simulation. A better approach is to determine the droplet size distribution using measurement data.

In the previous work reported in [6, 22], experimental validation was done for flame shape and length respectively. The experimental images of the flame were obtained using Schlieren photographs and it was shown that the flame shape was ”vee”, similar to that obtained for the Rosin-Rammler distribution reported here.

CONCLUSIONS AND FUTURE WORK

This paper successfully reports the development of an atomization model based on measurement data for a hollow-cone pressure swirl atomizer. The determined atomization model, which is based on the Rosin-Rammler distribution for droplets size is implemented in the Fluent solver for the simulation of liquid fuel combustion in a matrix burner. Cold flow and hot flow simulations results are reported and discussed.

Even though some useful results have been obtained, this is still work in progress. The following jobs are planned for the future:

1. Repeating the simulations for the droplet size distribution of droplets upto 100 μm and comparison of the cold flow mixing and the flames obtained using the two droplet size distributions.
2. Unsteady simulations of the flame based on the experimentally determined atomization model.
3. Study the effect of air-side forcing on the atomization process of the liquid droplets.
4. Further validation of the results with PDA measurements

ACKNOWLEDGMENT

The spray measurement data for the development of the atomization model have been provided by our cooperation partners Dr.-Ing. Diana Martin and Prof. Dr.-Ing. Reinhold Kneer from the Institute of Heat and Mass Transfer at the RWTH Aachen University. The authors gratefully acknowledge the financial support of the Deutsche Forschungsgemeinschaft (DFG) within the Collaborative Research Center (SFB) 686 ”Model based control of homogenized low-temperature combustion”. The responsibility of the content of this publication lies with the authors.

References

[1] Schuermans, B., Luebcke, H., Bajusz, D., and Flohr, P., 2005. “Thermoacoustic analysis of gas turbine combus-

tion systems using unsteady CFD". *Proceedings of ASME TURBO EXPO, Power for Land, Sea and Air, ASME Paper GT2005-6839, Reno-Tahoe, Nevada*, June 6-9.

[2] Bohn, D., Ohlendorf, N., Weidner, F., and Willie, J., 2010. "Active control of combustion instabilities in a matrix burner using primary and pilot fuel and acoustic forcing". *Proceedings of ASME TURBO EXPO, Power for Land Sea and Air, ASME Paper GT2010-23751, Glasgow, Scotland, UK*, June 14-18.

[3] Deuker, E., 1995. "Ein Beitrag zur Vorausberechnung des akustischen Stabilitätsverhaltens von Gasturbinen-Brennkammern mittels theoretischer und experimenteller Analyse von Brennkammerschwingungen". PhD thesis, Fakultät für Maschinenwesen der RWTH Aachen. Published in VDI Verlag, Energietechnik, Reihe 6, Nr. 317.

[4] Bohn, D., and Deuker, E., 1993. "An acoustical model to predict combustion driven oscillations". *20^{th} International Congress on Combustion Engines*.

[5] Bohn, D., Ohlendorf, N., and Willie, J., 2009. "Phase shift control of combustion instability in a gas turbine matrix burner using acoustic forcing and pulsed fuel injection". *Proceedings of ASME TURBO EXPO, Power for Land Sea and Air, ASME Paper GT2009-59083, Orlando, Florida, USA*, June 8-12.

[6] Bohn, D., Willie, J., and Ohlendorf, N., 2009. "Experimental and numerical studies of diesel spray evaporation and combustion in a gas turbine matrix burner". *Proceedings of ASME TURBO EXPO, Power for Land Sea and Air, ASME Paper GT2009-59348, Orlando, Florida, USA*, June 8-12.

[7] Lacas, F., 2005. Spray combustion. Tech. rep., Laboratoire EM2C du CNRS et de l'ECP, France.

[8] Peters, N., 2000. *Turbulent combustion: The state of the art*. Cambridge University Press, May.

[9] Faeth, G., 1983. "Evaporation and combustion of sprays". *Programme in Energy and Combustion Sci.,* ***9***(1).

[10] Sinnamon, J., Lancaster, D., and Steiner, J., 1980. "An experimental and analytical study of engine fuel spray trajectories". *SAE Paper 800135*.

[11] Hallman, M., Scheurlen, M., and Wittig, S., 1995. "Computation of turbulent evaporating sprays: Eulerian versus Langrangian approach". *J. of Engineering for Gas Turbines and Power,* ***117***, pp. 112–119.

[12] Chen, C., and Veshagh, A., 1993. "A simple unified fuel spray model". *SAE Paper 930923*.

[13] Wan, Y., and Peters, N., 1999. "Scaling of spray penetration with evaporation". *Atom. Sprays,* ***9***, pp. 111–132.

[14] Dukowicz, J., 1980. "A particle-fluid numerical model for liquid sprays". *J. of Computational Physics,* ***35***, pp. 229–253.

[15] Crowe, C., 1982. "Review-Numerical models for dilute gas-particle flows". *J. of Fluid Eng.,* ***104***(297).

[16] Gosman, A., and Ioannides, E., 1983. "Aspects of computer simulation of liquid-fueled combustors". *J. of Energy,* ***7***(482).

[17] Shuen, J., Solomoa, A., and Faeth, G., 1986. "Drop-turbulence interactions in diffusion flame". *AIAA J.,* ***24***(101).

[18] Lefebvre, A., 1983. *Atomization and sprays*. McGraw-Hill.

[19] Martin, D., 2009. Visualization and PDA for a stationary working pressure swirl atomizer. Internal report, Institute of Heat and Mass Transfer, RWTH-Aachen University.

[20] Tseng, L.-K., Wu, P.-K., and Faeth, G., 1992. High speed multiphase mixing layers. Unclassified report, Department of Aerospace Enginering, University of Michigan, Ann Arbor.

[21] Lefebvre, A., 1983. *Gas turbine combustion*. McGraw-Hill Series in Energy, Combustion, and Environment. McGraw-Hill.

[22] Bohn, D., Willie, J., and Ohlendorf, N., 2008. "Thermoacoustic modeling and transfer functions determination for a matrix burner using unsteady CFD". *Proceedings of ASME TURBO EXPO, Power for Land Sea and Air, ASME Paper GT2008-50370, Berlin, Germany*, June 9-13.